PKA-RIIB Deficiency Induces Brown Fatlike Adipocytes in Inguinal WAT and Promotes Energy Expenditure in Male FVB/NJ Mice

Jing Su,[1]* Wei Wu,[1]* Shan Huang,[1]* Ruidan Xue,[1] Yi Wang,[1] Yun Wan,[1] Lv Zhang,[1] Lang Qin,[1] Qiongyue Zhang,[1] Xiaoming Zhu,[1] Zhaoyun Zhang,[1] Hongying Ye,[1] Xiaohui Wu,[2] and Yiming Li[1]

[1]Department of Endocrinology and Metabolism, Huashan Hospital, and [2]Institute of Developmental Biology and Molecular Medicine, School of Life Sciences, Fudan University, Shanghai, 200433, China

Obesity has become the most common metabolic disorder worldwide. Promoting brown adipose tissue (BAT) and beige adipose tissue formation, and therefore, a functional increase in energy expenditure, may counteract obesity. Mice lacking type IIβ regulatory subunit of adenosine 3′,5′ cyclic monophosphate (cAMP)–dependent protein kinase A (PKA-RIIB) display reduced adiposity and resistance to diet-induced obesity. PKA-RIIB, encoded by the *Prkar2b* gene, is most abundant in BAT and white adipose tissue (WAT) and in the brain. In this study, we show that mice lacking PKA-RIIB have increased energy expenditure, limited weight gain, and improved glucose metabolism. PKA-RIIB deficiency induces brownlike adipocyte in inguinal WAT (iWAT). PKA-RIIB deficiency also increases the expression of uncoupling protein 1 and other thermogenic genes in iWAT and primary preadipocytes from iWAT through a mechanism involving increased PKA activity, which is represented by increased phosphorylation of PKA substrate, cAMP response element binding protein, and P38 mitogen-activated protein kinase. Our study provides evidence for the role of PKA-RIIB deficiency in regulating thermogenesis in WAT, which may potentially have therapeutic implications for the treatment of obesity and related metabolic disorders. **(*Endocrinology* 158: 578–591, 2017)**

Obesity develops when energy intake exceeds energy expenditure (EE) (1). Therefore, increasing EE in key metabolic organs, such as adipose tissue, has emerged as a potential and attractive strategy to prevent obesity (2). Adipose tissue, best known for its role in fat storage, can also suppress weight gain and metabolic diseases through the action of specialized, heat-producing adipocytes (brown adipocytes) (2). It has been recently established that substantial depots of uncoupling protein 1 (UCP1) expressing brownlike adipocytes can be detected in the supraspinal, supraclavicular, pericardial, and neck regions of adult humans (3–5). These adipocytes have been named "beige" or "brite" adipocytes. Under basal conditions, beige adipocytes express little to no UCP1, but UCP1 induction in response to cold promotes thermogenesis and EE (6). This process is generally called "browning." In several rodent models, browning of white adipose tissue (WAT) appears to be protective against diet-induced metabolic disorders, including obesity and diabetes (7–9). In human studies, the abundance of beige adipocytes is diminished in older and obese subjects (10, 11). Understanding the molecular processes governing WAT browning is highly important because this may uncover novel approaches for increasing EE and combating obesity and the metabolic syndrome.

ISSN Print 0013-7227 ISSN Online 1945-7170
Printed in USA

Received 15 August 2016. Accepted 2 December 2016.
First Published Online 14 December 2016

*These authors contributed equally to this study.

Abbreviations: BAT, brown adipose tissue; cAMP, adenosine 3′,5′ cyclic monophosphate; CNS, central nervous system; CREB, cAMP response element binding protein; EE, energy expenditure; eWAT, epididymal white adipose tissue; FBS, fetal bovine serum; HFD, high-fat diet; iWAT, inguinal white adipose tissue; KO, knockout; MAPK, mitogen-activated protein kinase; mRNA, messenger RNA; mtDNA, mitochondrial DNA; NCD, normal chow diet; PB, *Prkar2b*$^{PB/PB}$; PCR, polymerase chain reaction; PKA, protein kinase A; PKA-RIIB, type IIβ regulatory subunit of cAMP–dependent protein kinase A; RT, room temperature; TH, tyrosine hydroxylase; TNZ, thermoneutral zone; UCP1, uncoupling protein 1; VO_2, oxygen consumption; WAT, white adipose tissue; WT, wild type.

Adenosine 3′,5’ cyclic monophosphate (cAMP)–dependent protein kinase A (PKA) plays an important role in activating thermogenesis (2, 12). Active PKA can drive transcriptional responses in brown adipocyte through the activity of phosphorylated cAMP response element binding protein (CREB) and P38 mitogen-activated protein kinase (MAPK) (12). The inactive kinase holoenzyme is a tetramer that is composed of 2 regulatory and 2 catalytic subunits. cAMP causes the dissociation of the inactive holoenzyme into a dimmer of regulatory subunits bound to 4 cAMP and 2 free monomeric catalytic subunits. Four different regulatory subunits and 2 catalytic subunits have been identified in the mouse (13). Type IIβ regulatory subunit (PKA-RIIB) encoded by *Prkar2b* is one of the regulatory subunits and is most abundant in brown adipose tissue (BAT), WAT, and the brain, with very limited expression elsewhere (14). Knockout (KO) studies suggest that mice lacking PKA-RIIB exhibit leanness and resistance to diet-induced obesity and consequently metabolic disorders (14, 15). The PKA-RIIB KO mice have upregulated UCP1 in BAT and increased EE (14). PKA-RIIB deletion in genetically obese mice (*ob/ob*) increases BAT function and EE, leading to a reduction in body weight gain (16). However, whether the browning of WAT is also activated in PKA-RIIB–deficient mice remains to be determined.

In this study, we report that the browning of both inguinal WAT (iWAT) and epididymal WAT (eWAT) is activated in *Prkar2b*$^{PB/PB}$ (PB) mice; in these mice, the PKA-RIIB is disrupted by insertion of *piggyBac* in the *Prkar2b* gene. Additionally, differentiated preadipocytes from the iWAT of the mutant mice exhibit increased expression of *Ucp1* and some other thermogenic genes. Upregulated phosphorylation of CREB and P38 MAPK is consistent with the increased browning in iWAT and preadipocytes from the mutant mice compared with those from their wild-type (WT) littermate controls. Our study demonstrates that disruption of PKA-RIIB could activate the browning of white adipocytes, providing theoretical evidence for the important role played by PKA-RIIB in regulating EE.

Methods

Chemicals and antibodies

The antibodies (Table 1) used for immunoblotting included anti-UCP1 (ab10983; Abcam, Cambridge, United Kingdom), anti–peroxisome proliferator-activated receptor γ coactivator 1-α (anti–PGC1α; ab54481; Abcam), anti–PKA-RIIB (ab75993; Abcam), anti–type I-α regulatory subunit of PKA (anti–PKA-RIA; no. 5675S; Cell Signaling Technology, San Antonio, TX), antiphospho-P38 MAPK (no. 4511; Cell Signaling Technology), antitotal-P38 MAPK (no. 9212; Cell Signaling Technology), antiphospho-PKA substrate (no. 9624S; Cell Signaling Technology), antitotal CREB (no. 4820S; Cell Signaling Technology), antiphospho-CREB (no. 4276S; Cell Signaling Technology), anti– tyrosine hydroxylase (anti-TH; AB152; EMD Millipore/Fisher Scientific, Waltham, MA), and anti–heat shock protein 90 (sc-7947; Santa Cruz Biotechnology, Dallas, TX). All of the other chemicals were purchased from Sigma Chemical/Sigma-Aldrich (St. Louis, MO), unless otherwise specified.

Animals

PB mice were generated on the Friend Virus B NIH Jackson (FVB/NJ) background and characterized as previously described (17) [Fig. 1(B) and 1(C)]. Mapping information for *piggyBac* insertions in *Prkar2b* [Fig. 1(A)] can be found in the PB mice database (idm.fudan.edu.cn/PBmice). Offspring tail-genomic DNA was extracted and genotyped by polymerase chain reaction (PCR) using 3 primers: (1) 5′TGAGACAGGCTTCA AAAGAACTCAG3′; (2) 5′CTGAGATGTCCTAAATGCACA GCG3′; and (3) 5′AGGTCTTTTCCCAGAATTTACCACG3′ [Supplemental Fig. 1(A)]. Mice were housed at 22°C ± 2°C, in 55% ± 5% relative humidity, and under a 12-hour light/dark cycle with free access to water and a normal chow diet (NCD) or 60 kcal% high-fat diet (HFD) (Research Diets, New Brunswick, NJ), unless otherwise indicated. Littermates fed on the HFD began receiving that diet at the age of 6 weeks. Mice were housed in groups (2 to 4 animals per cage), unless otherwise specified. All animal-related experiments were performed in accordance with the guidelines from the Institute of Developmental Biology and Molecular Medicine Institutional Animal Care and Use Committee.

Measurement of food intake and feeding efficiency

Measurement of food intake was performed in 12-week-old male littermates fed on the NCD and 14-week-old male littermates fed on the HFD when the mice were housed individually. Mean daily food consumption was determined by calculating the amount of food consumed at 24-hour intervals for 7 days. Food intake normalized by body weight of the mice was represented as feeding efficiency.

Determination of energy content in feces

For measurement of energy content in feces, mice were housed individually. Feces were collected for 24 hours and dried for 72 hours at 60°C. The energy density was determined through an adiabatic bomb calorimeter (calorimeter C 5000; IKA-Werke, Staufen, Germany), using benzoic acid as a standard. Results of energy content in feces used in statistical analysis have been normalized by fecal weight.

Indirect calorimetry and physical activity

Oxygen consumption (VO_2) and physical activity were determined for male mice at 12 weeks of age with the NCD and 14 weeks of age with the HFD using a Promethion Metabolic Screening system (FG250; Sable Systems International, North Las Vegas, NV), according to the manufacturer’s instructions. The animals were acclimated to the system for 20 to 24 hours, and measurements of VO_2 and exhaled carbon dioxide were performed during the next 48 hours. The mice were maintained individually at 24°C under a 12-hour light/dark cycle. Food and water were available *ad libitum*. Voluntary activity was derived

Table 1. Antibody Table

Protein Target	RRID	Manufacturer, Catalog No.	Species Raised in; Monoclonal or Polyclonal	Dilution (ICH)	Dilution (IB)
Ucp1	AB_2241462	Abcam, ab10983	Rabbit; polyclonal	1:1000	1:500∼1000
PGC1 α	AB_881987	Abcam, ab54481	Rabbit; polyclonal		1:1000
PKA RIIβ	AB_1524201	Abcam,ab75993	Rabbit; polyclonal		1:2000
p38 MAPK	AB_330713	CST, 9212	Rabbit; polyclonal		1:1000
Phospho-p38 MAPK	AB_2139682	CST, 4511	Rabbit; monoclonal		1:500
CREB	AB_1903940	CST, 4820S	Rabbit; monoclonal		1:1000
Phospho-CREB	AB_10544696	CST, 4276S	Rabbit; monoclonal		1:1000
Phospho-PKA substrate	AB_331817	CST, 9624S	Rabbit; monoclonal		1:1000
PKA RIA	AB_10695452	CST, 5675S	Rabbit; monoclonal		1:1000
Tyrosine Hydroxylase	AB_390204	Millipore, Ab152	Rabbit; polyclonal	1:500	1:1000
Hsp90	AB_2121235	Santa Cruz Biotechnology, sc-7947	Rabbit; polyoclonal		1:1000

from the *x*-axis beam breaks, which were monitored every 15 minutes.

Body fat measurement

Body fat mass and lean mass were measured in conscious mice using a nuclear magnetic resonance instrument (minispec Body Composition Analyzer; Bruker, Billerica, MA). Mice were then euthanized with CO_2, and the subcutaneous (inguinal) and visceral (epididymal) fat pads were dissected bilaterally and their weights were recorded.

Determination of serum total cholesterol and triglyceride

Total cholesterol and triglyceride levels were assessed in the serum after a 4-hour fast enzymatically by automatic biochemistry (Cobas C501+6000; Roche Diagnostics, Risch-Rotkereuz, Switzerland) in the Center for Drug Safety Evaluation and Research, Shanghai Institute of Materia Medica, Chinese Academy of Sciences.

Intraperitoneal glucose tolerance test and insulin tolerance test

A glucose tolerance test was performed in male littermates after an overnight fast (16 to 18 hours). The glucose concentrations were measured in blood collected by venous bleeding from the tail vein immediately before and 15, 30, 60, 90, and 120 minutes after an intraperitoneal injection of 20% glucose saline solution (2 mg glucose per gram of body weight). An insulin tolerance test was performed in 6-hour (8:00 AM to 2:00 PM) fasting mice. The glucose concentrations were measured by venous bleeding at 0, 15, 30, 60, 90, and 120 minutes after an intraperitoneal injection of human insulin (Eli Lilly, Indianapolis, IN) at 0.5 or 0.75 mU/g for 12-week-old male mice fed on the NCD or 14-week-old male mice fed on the HFD, respectively.

Isolation of stromal vascular fractions and *in vitro* differentiation

Primary inguinal white fat stromal vascular fraction was obtained by collagenase I digestion from 4- to 6-week-old male FVB/NJ mice, according to the published methods described elsewhere (18). Primary stromal vascular cells were maintained in Dulbecco's modified Eagle's medium (F12) with 10% fetal bovine serum (FBS; Invitrogen, Carlsbad, CA) at 37°C in a 5% CO_2 environment. Adipocyte differentiation was induced in preadipocyte cultures by treating confluent cells for 48 hours in a medium containing 10% FBS, 0.5 mM isobutylmethylxanthine, 125 μm indomethacin, 2 μg/mL dexamethasone, 5 μg/mL insulin, and 1 nM triiodothyronine with 1 μm rosiglitazone. After 48 hours, the cells were moved to the medium containing 10% FBS, 5 μg/mL insulin, and 1 nM triiodothyronine with 1 μm rosiglitazone. Cells were harvested at day 8 after differentiating.

Histology and immunohistochemistry

Tissues fixed in 4% paraformaldehyde were sectioned after being paraffin embedded. Multiple sections were prepared and stained with hematoxylin and eosin for general morphological observations. Immunohistochemistry staining was performed according to the standard protocol using UCP1 and TH antibodies. Incubation was performed overnight in a humidified chamber at 4°C. The secondary antibodies for immunohistochemistry staining were purchased from Santa Cruz Biotechnology.

Oil red O staining

Dishes were washed twice with phosphate-buffered saline and fixed with 10% formalin for 20 minutes at room temperature. The cells were washed twice in phosphate-buffered saline, stained for 30 minutes at 37°C with a filtered oil red O working solution (0.5% oil red O in isopropyl alcohol), and then washed twice with distilled water and visualized under an inverted microscope.

Quantitative real-time PCR analysis

The total RNA was prepared with the TRIzol (Thermo Fisher Scientific, Waltham, MA) method, according to the manufacturer's instructions. Complementary DNA was prepared from 1 μg of RNA using the Reverse Transcription System (Takara, Kyoto, Japan). Then, 2.5 μL of diluted complementary DNA was used in a 10-μL PCR reaction with SYBR Green Master Mix (AceQ; Vazyme Biotech, Nanjing, China). PCRs were run in triplicate for each sample and analyzed in the Light Cycler 480 Real-Time PCR System (Roche Diagnostics). The relative expressions of the messenger RNAs (mRNAs) were determined after each measurement had been normalized to the 18S RNA level acting as the internal control. All of the primers

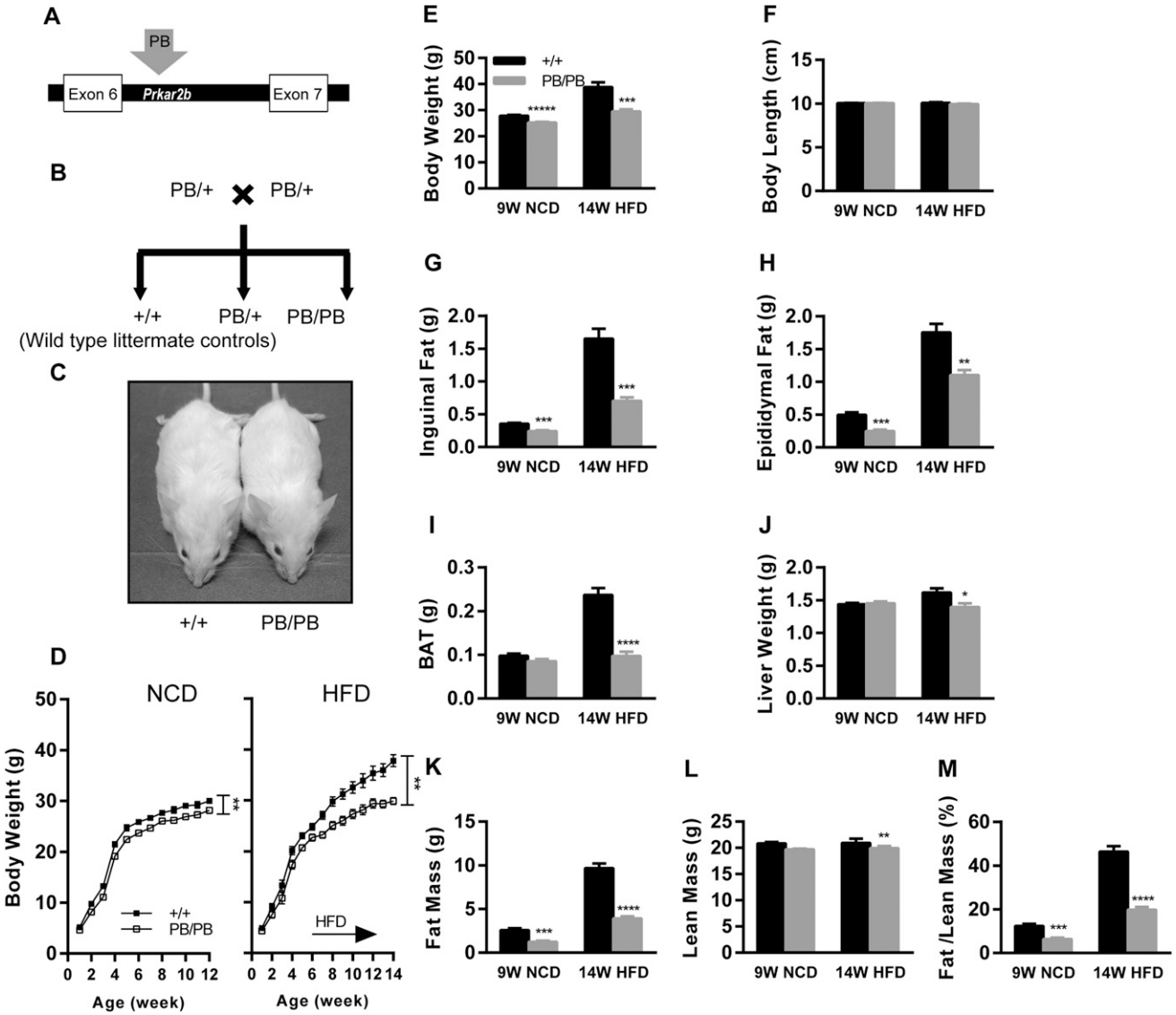

Figure 1. *Prkar2b*$^{PB/PB}$ mice are resistant to obesity. (A) Illustration of the position of *piggyBac* insertion in *Prkar2b*. The insertion was mapped between exon 6 and exon 7. (B) Breeding strategy for *Prkar2b*$^{PB/PB}$ mice (PB/PB) and their WT littermate controls ($^{+/+}$). (C) Photograph of 12-week-old male littermates of indicated *Prkar2b* genotypes. (D) Growth curves of male littermates fed on the NCD and HFD. The HFD was begun at 6 weeks of age. No. of mice: NCD $^{+/+}$, n = 11; NCD PB/PB, n = 11; HFD $^{+/+}$, n = 8; HFD PB/PB, n = 8. Data are represented as mean ± standard error of the mean (SEM) and were analyzed by 2-way analysis of variance for each diet (*$P < 0.05$; **$P < 0.01$; ***$P < 0.001$; **** $P < 0.0001$). (E) Body weight, (F) body length, (G) inguinal fat mass weight, (H) epididymal fat mass weight, (I) interscapular BAT mass weight, and (J) liver weight of male littermates fed on the NCD and HFD (n ≥ 6 for each genotype fed on each diet). Black bars, $^{+/+}$; gray bars, PB/PB. WT data served as statistical controls for each diet. The bar patterns of genotypes also apply to (K), (L), and (M). Data are represented as mean ± SEM and were analyzed by 2-tailed Student *t* test for each diet. (K) Fat mass weight, (L) lean mass weight, and (M) average fat/lean ratio of male littermates (n ≥ 8 for each genotype fed on each diet). Data are represented as mean ± SEM and were analyzed by 2-tailed Student *t* test for each diet.

were synthesized by Sangon Biotech (Shanghai, China). The sequences of the primers used in this study are listed in Supplemental Table 1.

Immunoblotting

Homogenized tissue and cells were lysed in radioimmunoprecipitation assay buffer containing protease and phosphatase inhibitors. The lysates were clarified by centrifugation at 12,000*g* for 10 minutes. The protein content of the supernatants was determined with a Protein Quantitative Analysis Kit (Thermo Fisher Scientific). Supernatants were boiled for 10 minutes at 100°C. The protein lysates were separated with sodium dodecyl (lauryl) sulfate-polyacrylamide gel electrophoresis and electroblotted to polyvinylidene fluoride (MilliporeSigma, Darmstadt, Germany). Electrophoresis supplies were from Bio-Rad Laboratories (Hercules, CA). The membranes were blocked and incubated with different antibodies, followed by incubation with horseradish peroxidase-conjugated secondary antibodies (Santa Cruz Biotechnology). Western blot analysis was conducted using enhanced chemiluminescence reagents (Thermo Fisher Scientific), according to the manufacturer's protocol.

Mitochondrial DNA content quantification by quantitative real-time PCR

Genomic DNA was isolated from WAT and BAT from PB and WT mice, respectively. The tissues were homogenized and digested with proteinase K at 55°C overnight in a lysis buffer for DNA extraction by a conventional phenol-chloroform method. The results were calculated from the difference in the threshold cycle values for mitochondrial DNA (mtDNA) and nuclear-specific amplification by quantitative real-time PCR. The data are expressed as mtDNA-specific 16S ribosomal RNA normalized to the nuclear specific gene *Sun1*. The sequences of the primers used in this study are listed in Supplemental Table 1.

Statistical analysis

All experiments were performed at least 3 times, and data are expressed as the mean ± standard error of the mean. GraphPad Prism (GraphPad Software, La Jolla, CA) was used for analysis of variance with 2-tailed Student *t* test and 2-way analysis of variance. $P < 0.05$ (2-tailed) was considered statistically significant.

Results

Prkar2b$^{PB/PB}$ mice are resistant to obesity

PB and WT mice were generated as depicted in Figure 1(B). Compared with WT mice, PB mice exhibited decreased body weight beginning at 3 weeks of age [Fig. 1(D)], and the HFD begun at 6 weeks of age amplified this difference [Fig. 1(D), right side]. Adult male PB mice exhibited significantly decreased body weight under both NCD and HFD [Fig. 1(E)]. Nuclear magnetic resonance analysis revealed that 9-week-old male PB mice receiving the NCD and 14-week-old male PB mice receiving the HFD had a dramatic decrease in body fat content [Fig. 1(K)] and fat/lean ratio [Fig. 1(M)], although their body length was unaltered [Fig. 1(F)]. PB mice receiving HFD exhibited significantly decreased lean mass [Fig. 1(L)]; however, compared with the decreasing in fat mass, the decreasing in lean mass is very small. Consistently, PB mice exhibited a marked decrease in inguinal and epididymal fat pad mass with both the NCD and HFD [Fig. 1(G) and (H)]. When fed on the HFD, WT mice exhibited dramatic lipid accumulation in liver and BAT [Supplemental Fig. 1(C) and 1(D)], which was almost completely prevented in PB mice. Meanwhile, liver weight and BAT weight were significantly lower in PB mice compared with WT mice [Fig. 1(I) and 1(J)]. These data indicate that PKA-RIIB disruption induces a decrease in adiposity and body weight.

Prkar2b$^{PB/PB}$ mice have improved glucose and lipids metabolism

Consistent with decreased body weight and body fat content, PB mice exhibited improved glucose tolerance, insulin sensitivity, and lipid metabolism.

We performed an intraperitoneal glucose tolerance test in 12-week-old male littermates receiving the NCD and 14-week-old male littermates receiving the HFD, respectively. After undergoing a 16-hour fast, PB mice showed lower fasting plasma glucose than WT mice [Fig. 2(B)]. After receiving an intraperitoneal injection of glucose, the plasma glucose levels of PB mice increased more slowly and cleared more quickly than those of WT mice [Fig. 2(A)], and this phenomenon was more obvious in mutants on the HFD than those on the NCD. Additionally, the area under the curve during the intraperitoneal glucose tolerance test in PB mice was lower than that of WT mice receiving both the NCD and HFD [Fig. 2(C)].

We analyzed the insulin sensitivity of 12-week-old male littermates on the NCD and 14-week-old male littermates on the HFD by performing an insulin tolerance test. PB mice receiving the HFD exhibited significantly more efficient glucose clearance upon receiving insulin [Fig. 2(D) and 2(F)], which indicates that the HFD could induce obesity-related insulin resistance in WT mice, but not PB mice.

Additionally, we examined the total cholesterol and triglyceride levels in serum of the mutants. Indeed, we observed that total cholesterol levels in PB mice were significantly lower than those of WT mice on both the NCD and HFD [Fig. 2(G)]. Triglyceride levels of PB mice were also lower than those of WT mice, but the significance was only observed in mice fed on the NCD, which may result from marked variation of mice fed on the HFD [Fig. 2(H)]. These data suggest that PB mice have the ability to resist obesity-related metabolic consequences.

PKA-RIIB disruption increases EE

A key factor for controlling energy homoeostasis is the balance between caloric intake and EE. We first examined the alteration in energy intake in PB mice by measuring food intake and fecal energy content. No significant alteration in food intake was observed in 12-week-old PB mice fed on the NCD or 14-week-old mice fed on the HFD [Fig. 3(A)]. The body weight–normalized food intake (feeding efficiency) also did not change in PB mice receiving either diet [Fig. 3(B)]. In addition, no difference in fecal energy content was found between PB and WT mice receiving either diet [Fig. 3(C)]. These data suggest that disrupting PKA-RIIB does not affect energy intake.

We then examined the alteration in EE of PB mice. We measured the 24-hour real-time EE of animals at the age of 12 weeks receiving the NCD and at the age of 14 weeks receiving the HFD, respectively, using the Promethion Metabolic Screening system (Sable Systems International). PB mice showed increased VO_2 and EE when receiving the NCD, and these differences

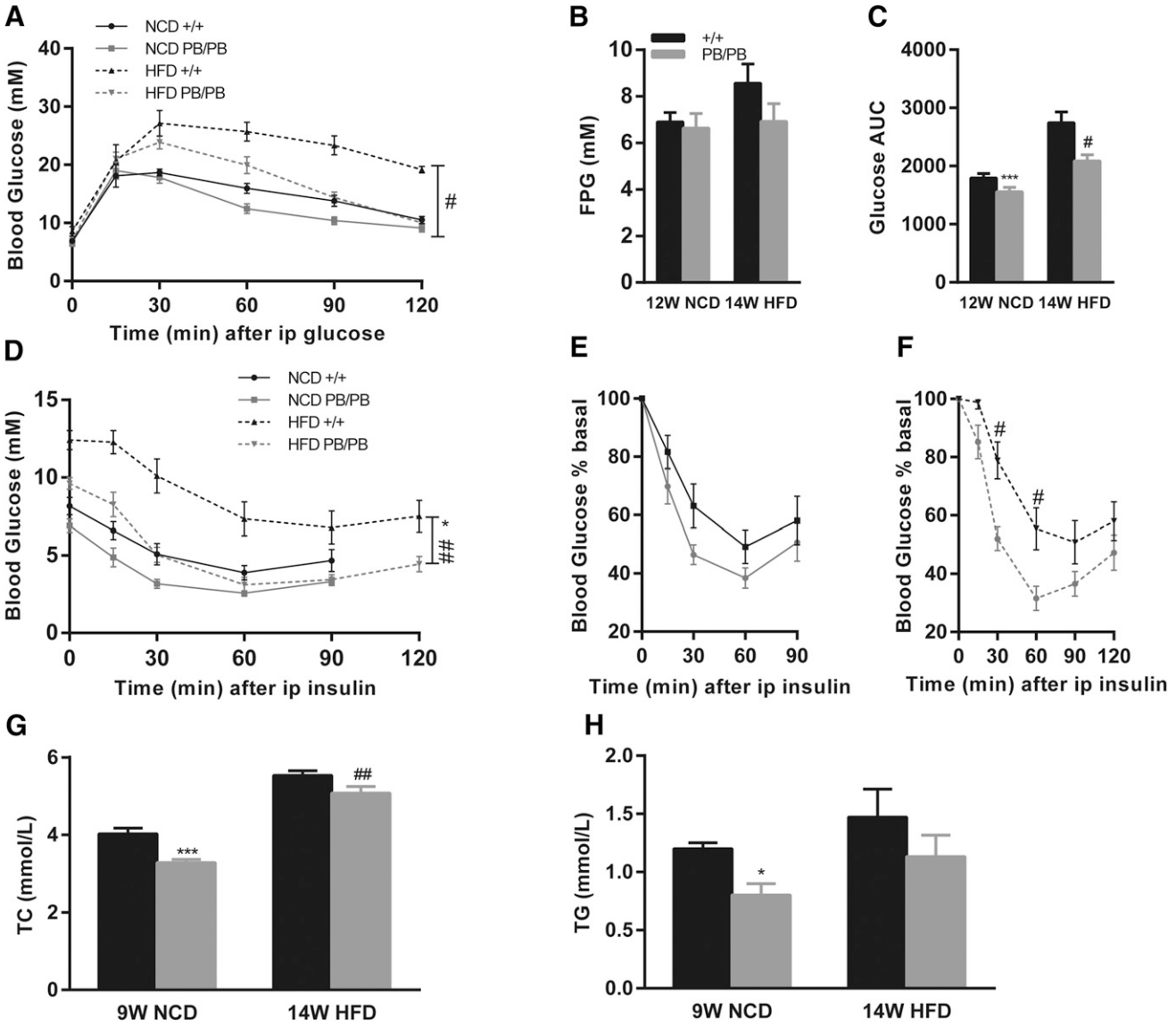

Figure 2. Disruption of PKA-RIIB improves glucose tolerance and lipids metabolism. (A) Glucose tolerance test results of 12-week-old male littermates fed on the NCD ($^{+/+}$, n = 6; PB/PB, n = 6) and 14-week-old male littermates fed on the HFD ($^{+/+}$, n = 5; PB/PB, n = 5). (B) Fasting plasma glucose (FPG) was determined after an overnight fast for 16 to 18 hours, and (C) glucose area under the curve (AUC) represents the average AUC. (D) Insulin tolerance test results of 12-week-old male littermates fed on the NCD ($^{+/+}$, n = 10; PB/PB, n = 10) and 14-week-old male littermates fed on the HFD ($^{+/+}$, n = 9; PB/PB, n = 9). FPG was determined after 1 day of fasting for 6 to 8 hours. Basal plasma glucose percentage of male littermates fed on (E) NCD and (F) HFD were calculated as the ratio of plasma glucose level at every time point to the blood glucose level of 0 minutes during the insulin tolerance test. (G) Serum total cholesterol (TC) and (H) serum triglyceride (TG) of 9-week-old male littermates fed on the NCD (n ≥ 6 for each group) and 14-week-old male littermates fed on the HFD (n ≥ 7 for each group). Difference in glucose level during (A) intraperitoneal glucose tolerance test and (D) insulin tolerance test between $^{+/+}$ and PB/PB mice was analyzed by 2-way analysis of variance for each diet. Analysis performed in figure parts (B), (C), and (E–H) was 2-tailed Student *t* test. Significant differences between $^{+/+}$ and PB/PB mice fed on NCD are indicated by *, and # indicates significant differences between $^{+/+}$ and PB/PB mice fed on HFD.

became significant in PB mice receiving the HFD [Fig. 3(E–H)]. Carbon dioxide release (VCO_2) and respiratory quotients were also evaluated [Supplemental Fig. 2(A–H)]. EE consists of physical activity, basal metabolism, and adaptive thermogenesis (19). Therefore, we evaluated physical activity of the mutants. PB mice exhibited slightly increased ambulatory movement, but the difference was not significant [Fig. 3(D)], which indicates that an alteration in physical activity does not contribute greatly to the lean phenotype of PB mice. Previous studies also suggest that physical activity changes in PKA-RIIB–deficient mice do not contribute markedly to the lean phenotype (20). These data indicate that increased thermogenesis may occur in the mutants.

No induction of UCP1 in BAT from *Prkar2b*$^{PB/PB}$ mice housed at room temperature

A previous study indicates that PKA-RIIB KO mice have an increase in UCP1 of BAT (14); thus, we investigated

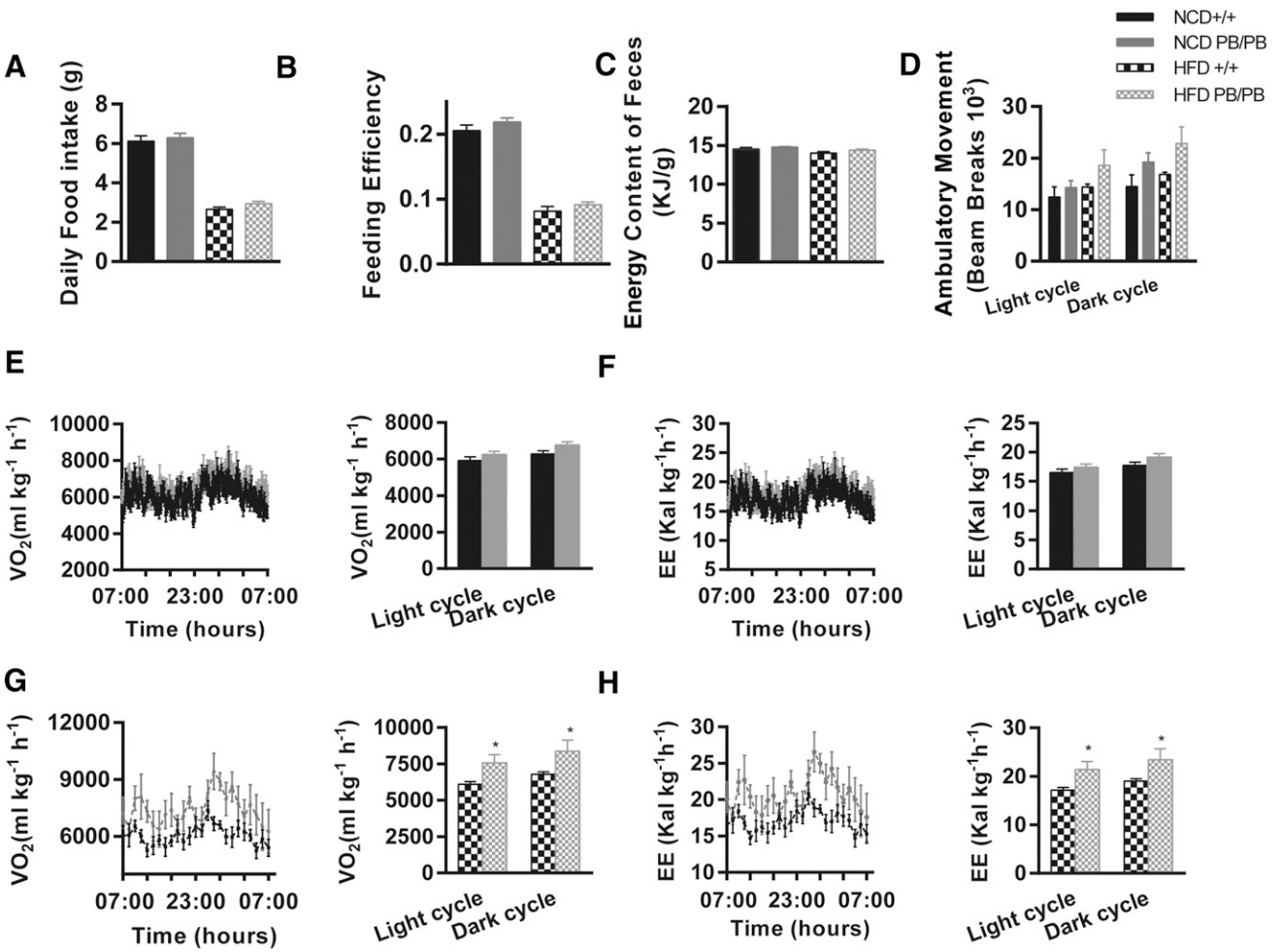

Figure 3. PKA-RIIB deficiency increases oxygen consumption and energy expenditure (EE). (A) Daily food intake, (B) feeding efficiency, (C) energy content of feces, and (D) ambulatory movement of 12-week-old male littermates fed on NCD and 14-week-old male littermates fed on HFD ($n \geq 6$ for each genotype fed on each diet). Feeding efficiency was calculated by dividing the daily food intake by body weight. The measurement of energy content of feces has been described in the methods section, and it indicates lipids absorption of mice. (E, F) EE was evaluated by measurement of VO_2 and carbon dioxide release (VCO_2) in 12-week-old male littermates fed on NCD and (G, H) 14-week-old male littermates fed on HFD. EE per animal was calculated as described in the methods section. EE, expressed as kcal $kg^{-1}h^{-1}$, has been normalized by body weight. Adjacent bar graphs represent the average for each group. Values represent mean ± standard error of the mean (SEM); error bars represent SEM, and significant differences between $^{+/+}$ and PB/PB mice fed on HFD are indicated by * (assessed by Student *t* test).

alterations in BAT from PB mice at the age of 9 weeks. No obvious morphological change was found in adipocytes in BAT from PB mice [Supplemental Fig. 3(A)]. Meanwhile, neither UCP1 nor PGC1α was upregulated [Supplemental Fig. 3(B)]. No change in mRNA level of *Ucp1* or *Pgc1α* was observed in the mutant BAT [Supplemental Fig. 3(D)]. Mitochondrial biogenesis as determined by mtDNA copy number was upregulated in BAT from PB mice; however, the difference was not significant [Supplemental Fig. 3(C)]. Consistently, the expression of mitochondrial synthesis and oxidation-related genes was not upregulated in BAT from PB mice [Supplemental Fig. 3(D)]. In addition, no obvious alteration was observed in PKA activity and the phosphorylation of P38 and CREB from the mutant BAT [Supplemental Fig. 3(E) and 3(F)]. All of these data were obtained from mice housed at room temperature (RT; 22°C), which is the industry-standard temperature considered to activate BAT and beige adipose. We intended to observe thermogenesis in the mutant BAT in the thermoneutral zone (TNZ; 30°C), which suppresses sympathetic tone and BAT-induced thermogenesis in mice (21). Male littermates at the age of 8 to 10 weeks were housed in the TNZ for 1 week. Interestingly, the level of UCP1 in BAT from PB mice was significantly higher than that from WT mice under TNZ conditions [Supplemental Fig. 3(G)]. However, there was no significant difference in mRNA level of *Ucp1* from BAT of PB vs WT mice [Supplemental Fig. 3(H)]. The mtDNA copy number was higher in BAT from PB mice than that from WT mice; however, the difference was not significant [Supplemental Fig. 3(I)].

Induced browning of inguinal WAT in *Prkar2b*$^{PB/PB}$ mice

Results in BAT induced us to investigate whether PKA-RIIB deficiency could promote browning in WAT. We observed alterations in iWAT from PB mice housed at RT at the age of 9 weeks . Reduced iWAT mass [Fig. 1(G)] was consistent with smaller adipocyte size [Fig. 4(A), upper panel] in PB mice. As shown in Figure 4(A) (lower panel), by performing UCP1 immunohistochemistry, we determined that the iWAT of PB mice was accompanied by a profound morphological transformation toward a BAT-like phenotype, which is observed in numerous clusters of UCP1 expressing multilocular adipocytes under basal conditions. Immunoblotting analysis showed that iWAT from PB mice had higher levels of specific BAT proteins such as UCP1 and PGC1α [Fig. 4(B)]. Mitochondrial biogenesis was fourfold

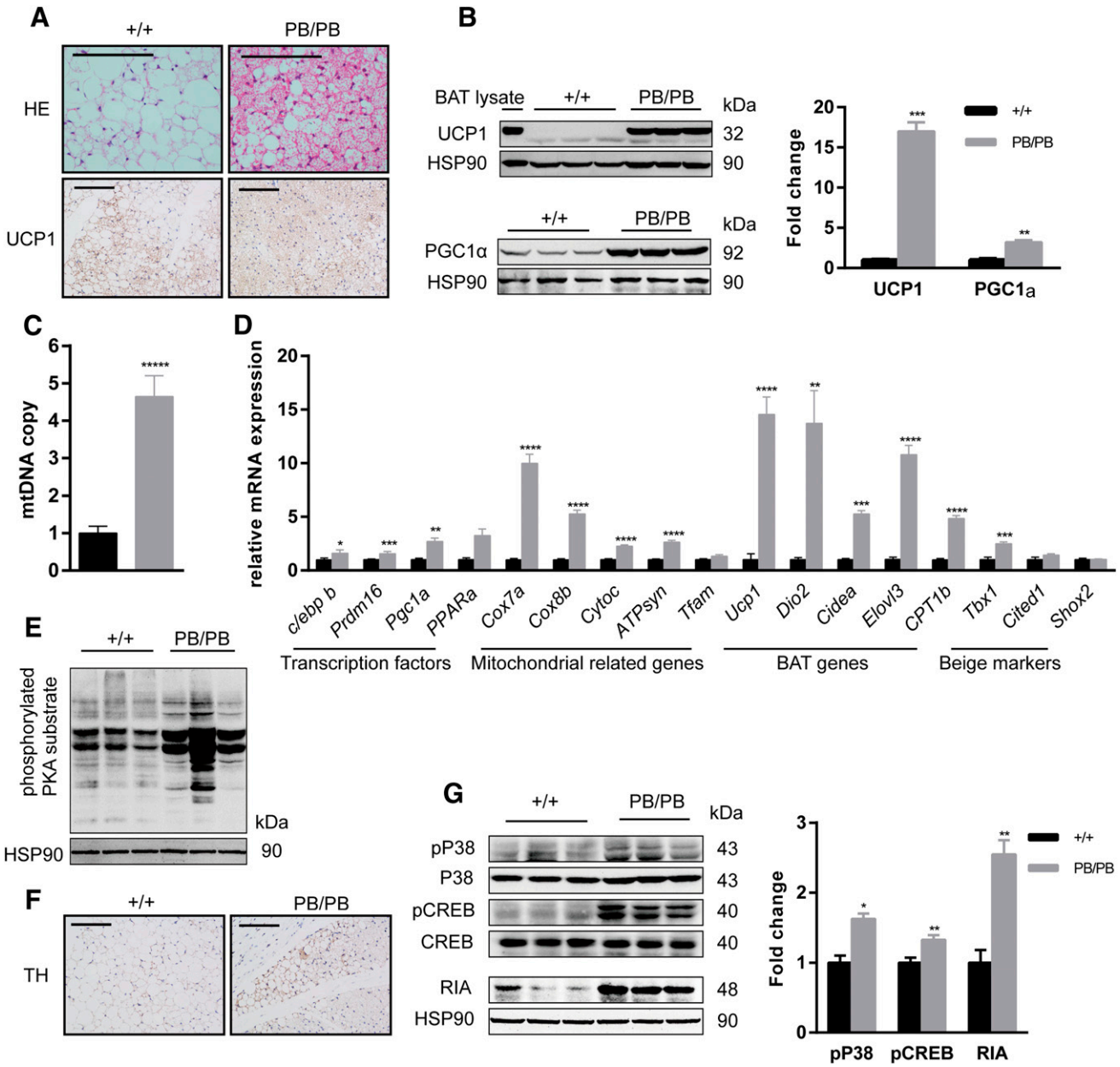

Figure 4. Disruption of PKA-RIIB–induced browning of iWAT. (A) Representative hematoxylin and eosin (HE) staining (upper panel) and immunohistochemistry for UCP1 (lower panel) in iWAT sections. Scale bar is 100 μm. (B) Immunoblotting showing UCP1 and PGC1α levels in iWAT (n = 3 for each genotype). BAT lysate was used as positive control for UCP1. Adjacent bar graph is the quantitative comparison. (C) Real-time PCR analysis revealing mtDNA copy number in iWAT. (D) Real-time PCR analysis revealing thermogenic gene expression in iWAT (n ≥ 8 for each genotype). (E) Immunoblotting showing phosphorylated PKA substrate level in iWAT (n = 3 for each genotype). (F) Immunohistochemistry for TH in iWAT sections. Scale bar is 100 μm. (G) Immunoblotting showing pP38, pCREB, and PKA-RIA levels in iWAT (n = 3 for each genotype). Adjacent bar graph is the quantitative comparison. All sections and samples were extracted from 9-week-old male littermates on the NCD housed at room temperature. Values represent mean ± standard error of the mean (SEM), error bars represent SEM, and significant differences compared with $^{+/+}$ mice are indicated by * (assessed by Student *t* test). HSP90, heat shock protein 90; pP38, phospho-P38 MAPK; pCREB, phospho-CREB.

higher in iWAT from PB mice than that from WT mice [Fig. 4(C)]. Consistently, the expression of mitochondrial-related genes was markedly increased in iWAT from PB mice compared with WT mice. Increased expression of key transcription factors related to thermogenesis, BAT markers, and beige markers occurred in iWAT from PB mice [Fig. 4(D)]. Then, we used an antiphosphorylated PKA substrate antibody to evaluate the activity of PKA in iWAT from PB mice, which could reflect the actual PKA activity *in vivo*. In iWAT from PB mice, we observed an increase in the level of phosphorylated PKA substrate [Fig. 4(E)], which could be the result of increased sympathetic outflow to iWAT and increased activity of PKA holoenzyme in adipose tissue. We next investigated the sympathetic input to adipose tissue by evaluating the level of TH, which is the rate-limiting enzyme in catecholamine synthesis and a marker of sympathetic innervations (22). TH was elevated in the iWAT from PB mice [Fig. 4(F)], suggesting that PKA-RIIB deficiency may augment the sympathetic input to iWAT and activate browning. Additionally, we found an increase in PKA-RIA [Fig. 4(G)]. PKA-RIA almost entirely replaces lost PKA-RIIB in mutant mice, in which an isoform switch from PKA type II to PKA type I is generated (14). PKA type I is considered to be more easily activated than PKA type II under basal conditions; thus, the isoform switch indicates increased basal activity (14). Consistent with the increased phosphorylated PKA substrate, we observed increased phosphorylation levels of P38 MAPK and CREB [Fig. 4(G)], both of which are key proteins in the downstream of PKA and have been established to be key elements in promoting UCP1 expression (2). These results indicate that the thermogenesis in iWAT from PB mice is activated under RT conditions. We also observed iWAT under TNZ conditions, and the activated thermogenesis in iWAT from PB mice was not suppressed by the TNZ [Supplemental Fig. 4(A–C)]. Additionally, increased thermogenesis was also observed in PB mice fed on HFD [Supplemental Fig. 4(D–G)].

Induced browning of epididymal WAT in *Prkar2b*$^{PB/PB}$ mice

The inguinal fat pad represents subcutaneous fat, whereas the epididymal fat pad represents visceral fat (23). The propensity to accumulate beige cells might be different between the 2 kinds of WAT deposits. Therefore, we investigated alterations in eWAT from PB mice at the age of 9 weeks housed in RT conditions as well. PKA-RIIB deficiency dramatically upregulated the mRNA level of *Ucp1* in eWAT [Fig. 5(D)], and the size of adipocytes in eWAT from PB mice were smaller than those from WT mice [Fig. 5(A), upper panel]. An increase in phosphorylated PKA substrate was observed in eWAT from PB mice [Fig. 5(E)]. Consistently, increased phosphorylation levels of P38 MAPK and CREB were observed [Fig. 5(F)]. However, morphological brown-like adipocytes were not seen in eWAT [Fig. 5(A), lower panel], and UCP1 could not be detected by immunoblotting in either group [Fig. 5(B)]. Except for *Ucp1*, only 2 thermogenic genes (*Dio2* and *Elovl3*) were upregulated in the eWAT from PB mice [Fig. 5(D)], and mitochondrial biogenesis was not changed in PB mice [Fig. 5(C)]. These results suggest that PKA-RIIB deficiency induces thermogenesis in the absence of morphological brownlike adipocytes in eWAT.

PKA-RIIB deficiency upregulated thermogenesis in primary white adipocytes

The increased thermogenesis in iWAT from PB mice seems to be the result of interaction between the increased sympathetic outflow to iWAT and the increased level of PKA-RIA. Increased sympathetic input in iWAT has been established to be associated with increased thermogenesis in iWAT (2); however, we were also interested in whether PKA-RIIB deficiency could induce thermogenesis by induction of PKA-RIA through cell autonomous mechanisms. Therefore, to investigate whether all of the alterations in gene expression that were observed in mutant iWAT could mediate by a direct effect, fractionated and differentiated primary iWAT adipocytes from 4- to 6-week-old male PB and WT mice were tested [Fig. 6(A) and 6(D)]. We observed a strong activation in BAT marker genes (*Pgc1α* and *Ucp1*), transcription factors (*Prdm16* and *c/ebp b*), and beige markers (*Cd137* and *Tbx1*) in primary iWAT adipocytes from the mutants [Fig. 6(E)]. Mitochondrial content [Fig. 6(C)], PGC1α, and UCP1 [Fig. 6(B)] were upregulated in the primary iWAT adipocytes from the mutant mice. Increased levels of phosphorylated PKA substrate and PKA-RIA were observed in primary iWAT adipocytes from the mutants [Fig. 6(F) and 6(G)], as well as the phosphorylation of P38 MAPK and CREB [Fig. 6(G)]. These results indicate that PKA-RIIB deficiency could promote thermogenesis by upregulating phosphorylative CREB and P38 MAPK through cell autonomous mechanisms.

Discussion

In this study, we observed resistance to diet-induced obesity, improved glucose metabolism, increased EE, and markedly upregulated browning of WAT in PKA-RIIB–deficient mice. PKA-RIIB exists in adipose tissue and the central nervous system (CNS). Disruption of PKA-RIIB resulted in increased sympathetic input in iWAT as well as upregulated phosphorylation of P38 MAPK and CREB in iWAT. In addition, primary pre-adipocytes in iWAT from PB mice exhibited increased

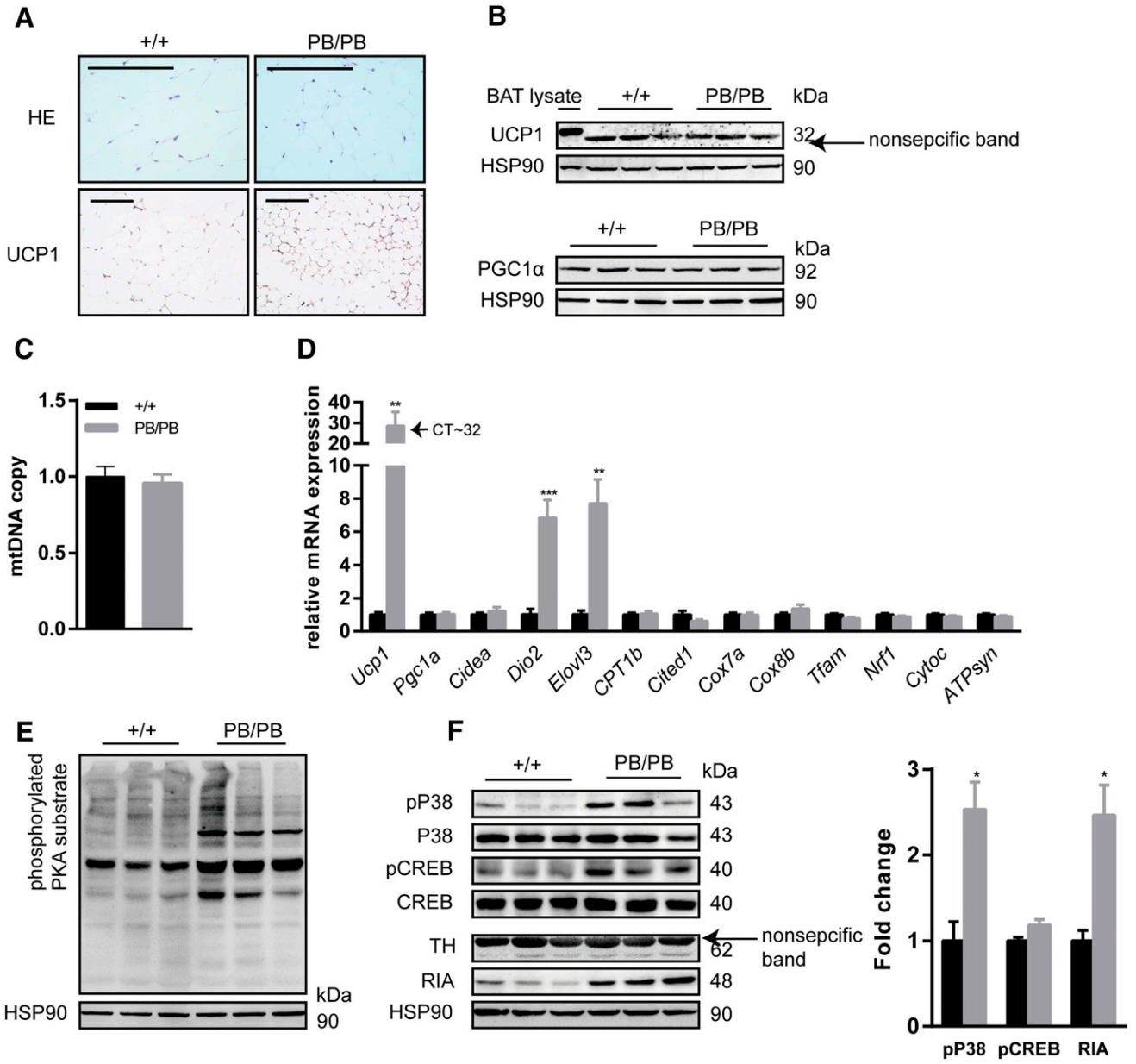

Figure 5. PKA-RIIB deficiency does not induce brownlike adipocytes in eWAT. (A) Representative hematoxylin and eosin (HE) staining (upper panel) and immunohistochemistry for UCP1 (lower panel) in eWAT sections. Scale bar is 100 μm. (B) Immunoblotting showing UCP1 and PGC1α levels in eWAT (n = 3 for each genotype). BAT lysate was used as positive control for UCP1. (C) Real-time PCR analysis revealing mtDNA copy number in eWAT (n ≥ 8 for each genotype). (D) Real-time PCR analysis revealing thermogenic gene expression in eWAT (n ≥ 8 for each genotype). (E) Immunoblotting showing phosphorylated PKA substrate level in eWAT (n = 3 for each genotype). (F) Immunoblotting showing pP38, pCREB, TH, and PKA-RIA levels in eWAT (n = 3 for each genotype). Adjacent bar graph is the quantitative comparison. All sections and samples were extracted from 9-week-old male littermates on the NCD housed at room temperature. Values represent mean ± standard error of the mean (SEM), error bars represent SEM, and significant differences in comparison with $^{+/+}$ mice are indicated by * (assessed by Student *t* test). HSP90, heat shock protein 90.

thermogenesis after being differentiated to be mature adipocytes compared with those from WT mice. Increased thermogenesis in WAT is considered to be associated with decreased body weight and improved metabolic state (2). Therefore, our study implies that PKA-RIIB deficiency may make a contribution to body weight loss by activating thermogenesis in WAT.

The increased thermogenesis in iWAT from PB mice may result from both alterations in the brain and adipocytes—in other words, increased thermogenesis is the result of interaction between the CNS and peripheral tissues. Recently, scientists reported hypersensitivity of leptin in hypothalamic γ-aminobutyric acid (GABA)ergic neurons in PKA-RIIB KO mice (24). Leptin action on GABAergic neurons reduces the inhibitory tone to proopiomelanocortin neurons (25), whereas hypersensitivity of leptin in proopiomelanocortin neurons is associated with upregulated sympathetic outflow to iWAT

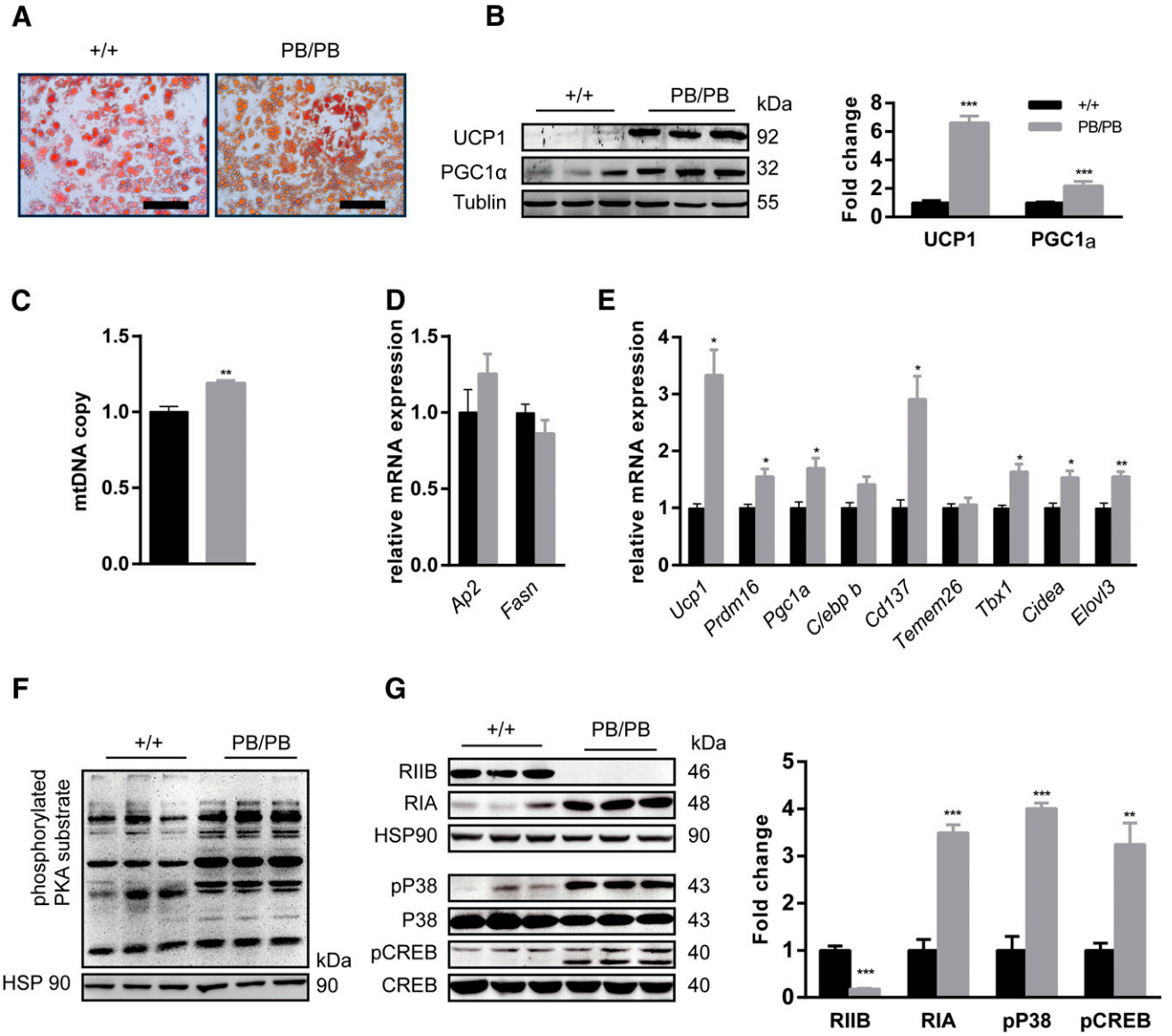

Figure 6. PKA-RIIB deficiency upregulated thermogenesis in differentiated stromal vascular fractions from iWAT. (A) Oil red O stain for primary iWAT adipocytes. Scale bar is 100 μm. (B) Immunoblotting showing UCP1 and PGC1α levels in primary iWAT adipocytes (n = 3 for each genotype). Adjacent bar graph is the quantitative comparison. (C) Real-time PCR analysis revealing mtDNA copy number in primary iWAT adipocytes (n = 3 for each genotype). Real-time PCR analysis revealing (D) differentiated related gene and (E) thermogenic gene expression in primary iWAT adipocytes (n = 4 for each genotype). (F) Immunoblotting showing phosphorylated PKA substrate level in primary iWAT adipocytes (n = 3 for each genotype). (G) Immunoblotting showing pP38, pCREB, PKA-RIIB, and PKA-RIA levels in primary iWAT adipocytes (n = 3 for each genotype); adjacent bar graph is the quantitative comparison. Primary iWAT adipocytes were obtained from 4- to 6-week-old male mice and differentiated as described in the Methods section. Values represent mean ± standard error of the mean (SEM), error bars represent SEM, and significant differences in comparison with $^{+/+}$ mice are indicated by * (Student *t* test). HSP90, heat shock protein 90.

(9). Administration of leptin to the hypothalamus can upregulate *Ucp1* mRNA expression in BAT and WAT through central modulation of sympathetic nervous system outflow (26). According to these previous studies, we speculate that leptin hypersensitivity in the hypothalamus may upregulate the browning of iWAT through an increase in sympathetic outflow in PB mice. Consistent with this speculation, we observed slightly increased expression of TH in iWAT from PB mice. Further investigation will be required to clarify whether the CNS takes control in inducing browning of iWAT in mutant mice, or whether this browning depends primarily on the sympathetic nervous system.

The interesting observation in our research is that PKA-RIIB deficiency in primary white preadipocytes can induce thermogenesis, whereas previous studies established that PKA-RIIB deficiency in adipose tissue does not contribute greatly to the lean phenotype of the mutant mice (20). Increased thermogenesis in white adipocytes has been established to be associated with decreased body weight and an improved metabolic state in many mice models; this topic has been reviewed before (2). However,

in some cases, the browning of WAT and a highly correlated improvement in glucose tolerance seem disproportional to the modest effect on body weight (7, 27). In other words, the ability of browning to improve glucose tolerance could be independent of body weight. Therefore, it is not precise to conclude that PKA-RIIB deficiency in adipocytes makes no contribution to an improved metabolic state, solely on the basis of the observation that it cannot result in markedly decreased body weight. In our study, isolated primary preadipocytes in iWAT from PB mice exhibited an increase in thermogenesis, which implies that disruption of PKA-RIIB in adipocytes may contribute to increased browning in iWAT. However, selective disruption of PKA-RIIB in adipose tissue is still needed to clarify whether PKA-RIIB deficiency in adipocytes is enough to induce increased browning of WAT and an improved metabolic state.

A precise mechanism whereby PKA-RIIB deficiency in white adipocytes results in increased thermogenesis remains to be determined. Our research *in vitro* indicates that PKA-RIIB deficiency could upregulate phosphorylation of CREB and P38 MAPK. These observations could be the result of the increased activity of PKA in adipocytes. In iWAT from PB mice, a compensatory increase in PKA-RIA replaces the loss of PKA-RIIB and results in an isoform switch from PKA type II to PKA type I (14, 28), which could result in the holoenzyme being more sensitive to cAMP and exhibiting higher activity. Recently, Dickson *et al.* (29) demonstrated that enhanced PKA activity in adipose tissue can induce UCP1 and improve metabolic health. In addition, increased PKA-RIA has also been reported to be associated with induction of browning in WAT in other studies (8, 30). However, we also found that an increased level of PKA-RIA is not always associated with increased PKA activity. For instance, the pathway downstream of PKA was not activated in BAT from PB mice in our study. The pathway downstream of PKA, represented by phosphorylation of CREB, exhibited an even lower level of activation in the hypothalamus of PKA-RIIB KO mice (24). Given that PKA type I is considered to be more easily activated than PKA type II under basal conditions, that observation demonstrates increased basal activity (14, 28). However, disruption of PKA-RIIB results in a decreased level of the catalytic subunit, which leads to decreased total PKA activity (14, 28). That is the reason that PKA extracted from mutant mice shows lower activity after treatment with a higher concentration of cAMP (14). Therefore, the actual activity of PKA *in vivo* is determined by the nature of the holoenzyme itself and the environment in which the enzyme is located. This speculation partly explains why we observed no increase in the level of phosphorylated PKA substrate in BAT from our PB mice, because different tissues have different concentrations of cAMP (31). Additionally, there may be some other mechanism whereby UCP1 was upregulated in WAT from PB mice. Consistent with our observation in BAT from PB mice, PKA-RIIB KO mice have an increase in UCP1 protein levels in BAT in the absence of an induction of *Ucp1* mRNA, which could be caused by either an increase in the synthesis or stability of the protein (32). This posttranscriptional effect may also exist in WAT of PB mice. Changes in PKA subunit composition may also alter PKA holoenzyme localization to specific signaling complexes, because PKA-RIIB has a much higher affinity for anchoring proteins than PKA-RIA (33).

Ucp1 mRNA was dramatically increased in eWAT from PB mice, although the levels of thermogenic gene expression were far lower in eWAT than in iWAT. However, PKA-RIIB deficiency can drive a program of brownlike adipocyte formation only in iWAT. The propensity to accumulate beige adipocyte might be different between the 2 kinds of WAT deposits. For instance, sympathetic input in iWAT is higher than that in eWAT (34), which makes iWAT more easily inducible to browning. Previous studies have reported that brown adipocytes can be induced in eWAT of transgenic animals in response to a strong pharmacological β-adrenergic stimulus (35). The increased expression of *Ucp1* in eWAT of PB mice may have been insufficient to induce a brownlike adipocyte formation in eWAT.

PKA-RIIB disruption induces an obvious browning in WAT; however, whether browning of WAT is primarily responsible for the leanness and the improved metabolic state of PB mice is unknown. This important question should be clarified in future studies. Nevertheless, our findings raise the intriguing possibility that downregulation of PKA-RIIB in adipose tissue may activate thermogenesis, a process that could potentially be used as therapy for obesity and related metabolic disorders. Use of mitochondrial uncoupling, for instance, with the chemical uncoupler 2,4-dinitrophenol, has been tried as a weight-loss therapy (36). However, upregulated respiratory uncoupling in all cells causes dangerous side effects (36). Thus, strategies that enhance respiratory uncoupling selectively in adipose tissue should be safe. Considering that PKA-RIIB is most abundant in adipose tissue and the CNS, creating small molecule drugs that target PKA-RIIB and cannot penetrate the blood-brain barrier may provide a potential safe therapy for type 2 diabetes mellitus and other metabolic disorders.

Acknowledgments

Address all correspondence and requests for reprints to: Yiming Li, MD, Department of Endocrinology and Metabolism,

Huashan Hospital, Fudan University, No.12 Middle Urumqi Road, Jing'an District, Shanghai, 200040, People's Republic of China. E-mail: yimingli_fudan@163.com.

This work was supported by the National Natural Science Foundation (Grants 81471083, 81070680, 81500673, and 81400844); as a scientific research project supported by Huashan Hospital, Fudan University (Grant 2013QD10); and by the Shanghai Municipal Commission of Health and Family Planning (Grant 20144Y0070).

Author contributions: J.S., W.W., and S.H. contributed equally to the study. J.S. researched data and wrote the manuscript. S.H. conceived and designed the experiment and researched data. W.W. researched data. L.Z., L.Q., Q.Z., and X.Z. contributed to the discussion. Y. Wan contributed to the cell experiment. R.X., Y. Wang, Z.Z., H.Y., and X.W. contributed to the discussion and reviewed the manuscript. Y.L. conceived and designed the experiment and took responsibility for the integrity of the data and the accuracy of the data analysis.

Disclosure Summary: The authors have nothing to disclose.

References

1. Lau DC, Douketis JD, Morrison KM, Hramiak IM, Sharma AM, Ur E; Obesity Canada Clinical Practice Guidelines Expert Panel. 2006 Canadian clinical practice guidelines on the management and prevention of obesity in adults and children [summary]. *CMAJ*. 2007;**176**(8):S1–S13.
2. Harms M, Seale P. Brown and beige fat: development, function and therapeutic potential. *Nat Med*. 2013;**19**(10):1252–1263.
3. van Marken Lichtenbelt WD, Vanhommerig JW, Smulders NM, Drossaerts JM, Kemerink GJ, Bouvy ND, Schrauwen P, Teule GJ. Cold-activated brown adipose tissue in healthy men. *N Engl J Med*. 2009;**360**(15):1500–1508.
4. Virtanen KA, Lidell ME, Orava J, Heglind M, Westergren R, Niemi T, Taittonen M, Laine J, Savisto NJ, Enerbäck S, Nuutila P. Functional brown adipose tissue in healthy adults. *N Engl J Med*. 2009;**360**(15):1518–1525.
5. Cypess AM, Lehman S, Williams G, Tal I, Rodman D, Goldfine AB, Kuo FC, Palmer EL, Tseng YH, Doria A, Kolodny GM, Kahn CR. Identification and importance of brown adipose tissue in adult humans. *N Engl J Med*. 2009;**360**(15):1509–1517.
6. Rosen ED, Spiegelman BM. What we talk about when we talk about fat. *Cell*. 2014;**156**(1-2):20–44.
7. Seale P, Conroe HM, Estall J, Kajimura S, Frontini A, Ishibashi J, Cohen P, Cinti S, Spiegelman BM. Prdm16 determines the thermogenic program of subcutaneous white adipose tissue in mice. *J Clin Invest*. 2011;**121**(1):96–105.
8. Cederberg A, Grønning LM, Ahrén B, Taskén K, Carlsson P, Enerbäck S. FOXC2 is a winged helix gene that counteracts obesity, hypertriglyceridemia, and diet-induced insulin resistance. *Cell*. 2001;**106**(5):563–573.
9. Dodd GT, Decherf S, Loh K, Simonds SE, Wiede F, Balland E, Merry TL, Münzberg H, Zhang ZY, Kahn BB, Neel BG, Bence KK, Andrews ZB, Cowley MA, Tiganis T. Leptin and insulin act on POMC neurons to promote the browning of white fat. *Cell*. 2015;**160**(1-2):88–104.
10. Lee P, Linderman JD, Smith S, Brychta RJ, Wang J, Idelson C, Perron RM, Werner CD, Phan GQ, Kammula US, Kebebew E, Pacak K, Chen KY, Celi FS. Irisin and FGF21 are cold-induced endocrine activators of brown fat function in humans. *Cell Metab*. 2014;**19**(2):302–309.
11. Ouellet V, Routhier-Labadie A, Bellemare W, Lakhal-Chaieb L, Turcotte E, Carpentier AC, Richard D. Outdoor temperature, age, sex, body mass index, and diabetic status determine the prevalence, mass, and glucose-uptake activity of 18F-FDG-detected BAT in humans. *J Clin Endocrinol Metab*. 2011;**96**(1):192–199.
12. Collins S. β-adrenoceptor signaling networks in adipocytes for recruiting stored fat and energy expenditure. *Front Endocrinol (Lausanne)*. 2012;**2**:102.
13. McKnight GS. Cyclic AMP second messenger systems. *Curr Opin Cell Biol*. 1991;**3**(2):213–217.
14. Cummings DE, Brandon EP, Planas JV, Motamed K, Idzerda RL, McKnight GS. Genetically lean mice result from targeted disruption of the RII beta subunit of protein kinase A. *Nature*. 1996;**382**(6592):622–626.
15. Schreyer SA, Cummings DE, McKnight GS, LeBoeuf RC. Mutation of the RIIbeta subunit of protein kinase A prevents diet-induced insulin resistance and dyslipidemia in mice. *Diabetes*. 2001;**50**(11):2555–2562.
16. Newhall KJ, Cummings DE, Nolan MA, McKnight GS. Deletion of the RIIbeta-subunit of protein kinase A decreases body weight and increases energy expenditure in the obese, leptin-deficient ob/ob mouse. *Mol Endocrinol*. 2005;**19**(4):982–991.
17. Ding S, Wu X, Li G, Han M, Zhuang Y, Xu T. Efficient transposition of the piggyBac (PB) transposon in mammalian cells and mice. *Cell*. 2005;**122**(3):473–483.
18. Aune UL, Ruiz L, Kajimura S. Isolation and differentiation of stromal vascular cells to beige/brite cells. *J Vis Exp*. 2013; (73).
19. Rosen ED, Spiegelman BM. Adipocytes as regulators of energy balance and glucose homeostasis. *Nature*. 2006;**444**(7121):847–853.
20. Zheng R, Yang L, Sikorski MA, Enns LC, Czyzyk TA, Ladiges WC, McKnight GS. Deficiency of the RIIβ subunit of PKA affects locomotor activity and energy homeostasis in distinct neuronal populations. *Proc Natl Acad Sci USA*. 2013;**110**(17):E1631–E1640.
21. Overton JM. Phenotyping small animals as models for the human metabolic syndrome: thermoneutrality matters. *Int J Obes*. 2010;**34**(Suppl 2):S53–S58.
22. Vaughan CH, Zarebidaki E, Ehlen JC, Bartness TJ. Analysis and measurement of the sympathetic and sensory innervation of white and brown adipose tissue. *Methods Enzymol*. 2014;**537**:199–225.
23. Bjørndal B, Burri L, Staalesen V, Skorve J, Berge RK. Different adipose depots: their role in the development of metabolic syndrome and mitochondrial response to hypolipidemic agents. *J Obes*. 2011;**2011**:490650.
24. Yang L, McKnight GS. Hypothalamic PKA regulates leptin sensitivity and adiposity. *Nat Commun*. 2015;**6**:8237.
25. Vong L, Ye C, Yang Z, Choi B, Chua S Jr, Lowell BB. Leptin action on GABAergic neurons prevents obesity and reduces inhibitory tone to POMC neurons. *Neuron*. 2011;**71**(1):142–154.
26. Commins SP, Watson PM, Levin N, Beiler RJ, Gettys TW. Central leptin regulates the UCP1 and ob genes in brown and white adipose tissue via different beta-adrenoceptor subtypes. *J Biol Chem*. 2000;**275**(42):33059–33067.
27. Boström P, Wu J, Jedrychowski MP, Korde A, Ye L, Lo JC, Rasbach KA, Boström EA, Choi JH, Long JZ, Kajimura S, Zingaretti MC, Vind BF, Tu H, Cinti S, Højlund K, Gygi SP, Spiegelman BM. A PGC1-α-dependent myokine that drives brown-fat-like development of white fat and thermogenesis. *Nature*. 2012;**481**(7382):463–468.
28. Amieux PS, Cummings DE, Motamed K, Brandon EP, Wailes LA, Le K, Idzerda RL, McKnight GS. Compensatory regulation of RIalpha protein levels in protein kinase A mutant mice. *J Biol Chem*. 1997;**272**(7):3993–3998.
29. Dickson LM, Gandhi S, Layden BT, Cohen RN, Wicksteed B. Protein kinase A induces UCP1 expression in specific adipose depots to increase energy expenditure and improve metabolic health. *Am J Physiol Regul Integr Comp Physiol*. 2016;**311**(1):R79–R88.
30. Dahle MK, Grønning LM, Cederberg A, Blomhoff HK, Miura N, Enerbäck S, Taskén KA, Taskén K. Mechanisms of FOXC2- and FOXD1-mediated regulation of the RI alpha subunit of cAMP-dependent protein kinase include release of transcriptional repression and activation by protein kinase B alpha and cAMP. *J Biol Chem*. 2002;**277**(25):22902–22908.

31. Hofmann F, Bechtel PJ, Krebs EG. Concentrations of cyclic AMP-dependent protein kinase subunits in various tissues. *J Biol Chem*. 1977;**252**(4):1441–1447.
32. Nolan MA, Sikorski MA, McKnight GS. The role of uncoupling protein 1 in the metabolism and adiposity of RII beta-protein kinase A-deficient mice. *Mol Endocrinol*. 2004;**18**(9):2302–2311.
33. Burton KA, Johnson BD, Hausken ZE, Westenbroek RE, Idzerda RL, Scheuer T, Scott JD, Catterall WA, McKnight GS. Type II regulatory subunits are not required for the anchoring-dependent modulation of Ca2+ channel activity by cAMP-dependent protein kinase. *Proc Natl Acad Sci USA*. 1997;**94**(20):11067–11072.
34. Murano I, Barbatelli G, Giordano A, Cinti S. Noradrenergic parenchymal nerve fiber branching after cold acclimatisation correlates with brown adipocyte density in mouse adipose organ. *J Anat*. 2009;**214**(1):171–178.
35. Seale P, Kajimura S, Yang W, Chin S, Rohas LM, Uldry M, Tavernier G, Langin D, Spiegelman BM. Transcriptional control of brown fat determination by PRDM16. *Cell Metab*. 2007;**6**(1):38–54.
36. Harper JA, Dickinson K, Brand MD. Mitochondrial uncoupling as a target for drug development for the treatment of obesity. *Obes Rev*. 2001;**2**(4):255–265.